Proceedings of the ASME/JSME 2011 8th Thermal Engineering Joint Conference
AJTEC2011
March 13-17, 2011, Honolulu, Hawaii, USA

AJTEC2011-44315

PREDICTING PHONON PROPERTIES FROM MOLECULAR DYNAMICS SIMULATIONS USING THE SPECTRAL ENERGY DENSITY

Joseph E. Turney
John A. Thomas
Alan J. H. McGaughey*
Department of Mechanical Engineering
Carnegie Mellon University
Pittsburgh, Pennsylvania 15213-3890
Email: mcgaughey@cmu.edu

Cristina H. Amon
Department of Mechanical Engineering
Carnegie Mellon University
Pittsburgh, Pennsylvania 15213-3890

Department of Mechanical & Industrial Engineering
University of Toronto
Toronto, Ontario M5S 3G8

ABSTRACT

Using lattice dynamics theory, we derive the spectral energy density and the relation between the spectral energy density and the phonon frequencies and relaxation times. We then calculate the spectral energy density and phonon frequencies and relaxation times for a test system of Lennard-Jones argon using velocities obtained from molecular dynamics simulations. The phonon properties, which can be used to calculate thermal conductivity, are compared to predictions made using (i) anharmonic lattice dynamics calculations and (ii) a technique that performs normal mode analysis on the positions and velocities obtained from molecular dynamics simulations.

INTRODUCTION

Due to the increasing prevalence of nanostructured electronic and optoelectronic devices and the desire to employ nanostructuring to tune material properties, it is vital to develop an understanding of the physics of carrier transport. Phonons are the dominant energy carriers in insulators and semiconductors, which are integral to many nanostructured devices. While substantial effort has gone into developing adequate theories of phonon transport, the current understanding is lacking, even in bulk materials. For example, which phonon modes dominate energy transport and the importance of interactions involving four or more phonons are typically unknown. The situation only becomes more complicated in nanostructures, where the energy carriers also interact with surfaces and interfaces.

The usefulness of analytical models of thermal transport has been hampered by the necessary approximations and assumptions (e.g., a Debye solid, ignoring optical phonons), permitting only qualitative or semi-quantitative predictions [1, 2]. When used with the Green-Kubo or direct methods, molecular dynamics (MD) simulations can predict thermal conductivity [3–6]. Because the analysis in these two methods is performed at the system level, however, no information about the phonons is obtained. The phonon properties needed to calculate thermal conductivity (group velocities, relaxation times) can be predicted using MD simulation and normal mode analysis [3, 7–9], but this method requires *a priori* knowledge of the phonon frequencies and polarization vectors and is time-intensive. Phonon frequencies and relaxation times can be obtained from harmonic and anharmonic lattice dynamics (LD) calculations, [7,10–13] but these are theoretically and computationally complex and only valid at low temperatures.

The spectral energy density (SED) [14–17], which we discuss herein, presents a straightforward alternative by which phonon frequencies and relaxation times can be obtained using only atomic velocities from an MD simulation as input. In what follows, we derive the SED from lattice dynamics theory. We also derive the relation between the SED and the phonon fre-

*Address all correspondence to this author.

quencies and relaxation times. We then calculate the SED using results from MD simulations of a test system of Lennard-Jones argon and compare the predicted phonon properties to predictions made using (i) anharmonic LD calculations and (ii) normal mode analysis performed on the results of the MD simulations.

THE SPECTRAL ENERGY DENSITY

Derivation

To derive the SED, we begin with results from standard harmonic LD theory. The system Hamiltonian is [18],

$$\begin{aligned} H =& \frac{1}{2}\sum_{\boldsymbol{\kappa},\nu}^{N,3n}\left[\dot{q}^*(\boldsymbol{\kappa};_\nu t)\,\dot{q}(\boldsymbol{\kappa};_\nu t)+\omega_0^2(\boldsymbol{\kappa};_\nu)\,q^*(\boldsymbol{\kappa};_\nu t)\,q(\boldsymbol{\kappa};_\nu t)\right] \\ =& \sum_{\boldsymbol{\kappa},\nu}^{N,3n}\left[T(\boldsymbol{\kappa};_\nu t)+V(\boldsymbol{\kappa};_\nu t)\right], \end{aligned} \tag{1}$$

where t is time, $\omega_0(\boldsymbol{\kappa};_\nu)$ is the frequency of the phonon denoted by wave vector $\boldsymbol{\kappa}$ and dispersion branch ν, and N and n are the total number of unit cells and number of atoms in the unit cell. The Hamiltonian is the total system energy and is the sum of the mode- and time-dependent kinetic and potential energies, $T(\boldsymbol{\kappa};_\nu t)$ and $V(\boldsymbol{\kappa};_\nu t)$. The phonon mode (normal mode) coordinate and its time derivative are given by

$$q(\boldsymbol{\kappa};_\nu t) = \sum_{\alpha,b,l}^{3,n,N}\sqrt{\frac{m_b}{N}}u_\alpha(_b^l;t)\,e^*(_\nu^{\boldsymbol{\kappa}}{}_\alpha^b)\exp\left[i\boldsymbol{\kappa}\cdot\mathbf{r}_0(_0^l)\right], \tag{2}$$

and

$$\dot{q}(\boldsymbol{\kappa};_\nu t) = \sum_{\alpha,b,l}^{3,n,N}\sqrt{\frac{m_b}{N}}\dot{u}_\alpha(_b^l;t)\,e^*(_\nu^{\boldsymbol{\kappa}}{}_\alpha^b)\exp\left[i\boldsymbol{\kappa}\cdot\mathbf{r}_0(_0^l)\right], \tag{3}$$

where m_b is the mass of the b^{th} atom in the unit cell, and $\mathbf{r}_0(_0^l)$ is the equilibrium position vector of the l^{th} unit cell. The α-component of the displacement (from equilibrium), $u_\alpha(_b^l;t)$, and velocity, $\dot{u}_\alpha(_b^l;t)$, of the b^{th} atom in the l^{th} unit cell are time-dependent and are related to the phonon mode coordinates through the time-independent polarization vector $e(_\nu^{\boldsymbol{\kappa}}{}_\alpha^b)$. The asterisk superscript in Eqs. (2) and (3) denotes the complex conjugate.

The allowed wave vectors are defined by the crystal lattice, however, the phonon frequencies and polarization vectors are not known. It is convenient to let $\sum_{\alpha,b}^{3,n} q(_\nu^{\boldsymbol{\kappa}}{}_\alpha^b;t) = q(\boldsymbol{\kappa};_\nu t)$ and recast Eqs. (1), (2), and (3) as

$$\begin{aligned} H =& \frac{1}{2}\sum_{\boldsymbol{\kappa},\nu}^{N,3n}\sum_{\alpha,b}^{3,n}\left[\dot{q}^*(_\nu^{\boldsymbol{\kappa}}{}_\alpha^b;t)\,\dot{q}(_\nu^{\boldsymbol{\kappa}}{}_\alpha^b;t)+\omega_0^2(_\nu^{\boldsymbol{\kappa}}{}_\alpha^b)\,q^*(_\nu^{\boldsymbol{\kappa}}{}_\alpha^b;t)\,q(_\nu^{\boldsymbol{\kappa}}{}_\alpha^b;t)\right] \\ =& \sum_{\boldsymbol{\kappa},\nu}^{N,3n}\sum_{\alpha,b}^{3,n}\left[T(_\nu^{\boldsymbol{\kappa}}{}_\alpha^b;t)+V(_\nu^{\boldsymbol{\kappa}}{}_\alpha^b;t)\right], \end{aligned} \tag{4}$$

$$q(_\nu^{\boldsymbol{\kappa}}{}_\alpha^b;t) = e(_\nu^{\boldsymbol{\kappa}}{}_\alpha^b)\sqrt{\frac{m_b}{N}}\sum_{l}^{N}u_\alpha(_b^l;t)\exp\left[i\boldsymbol{\kappa}\cdot\mathbf{r}_0(_0^l)\right], \tag{5}$$

and

$$\dot{q}(_\nu^{\boldsymbol{\kappa}}{}_\alpha^b;t) = e(_\nu^{\boldsymbol{\kappa}}{}_\alpha^b)\sqrt{\frac{m_b}{N}}\sum_{l}^{N}\dot{u}_\alpha(_b^l;t)\exp\left[i\boldsymbol{\kappa}\cdot\mathbf{r}_0(_0^l)\right]. \tag{6}$$

The coordinates $q(_\nu^{\boldsymbol{\kappa}}{}_\alpha^b;t)$ are associated with atom b and direction α. In arriving at Eq. (4), we make use of the fact that $e(_\nu^{\boldsymbol{\kappa}}{}_\alpha^b) = e^*(_\nu^{-\boldsymbol{\kappa}}{}_\alpha^b)$ and $q(\boldsymbol{\kappa};_\nu t) = q^*(-\boldsymbol{\kappa};_\nu t)$ [12] to pull the summations over α and b out of the multiplications in Eq. (1).

The average kinetic energy of the crystal is

$$\langle T(_\nu^{\boldsymbol{\kappa}}{}_\alpha^b;t)\rangle = \frac{1}{2}\lim_{\tau_0\to\infty}\frac{1}{2\tau_0}\int_{-\tau_0}^{\tau_0}\dot{q}^*(_\nu^{\boldsymbol{\kappa}}{}_\alpha^b;t)\,\dot{q}(_\nu^{\boldsymbol{\kappa}}{}_\alpha^b;t)\,dt. \tag{7}$$

The kinetic energy can be transformed from the time domain (t) to the frequency domain (ω) by Parseval's theorem [19], allowing Eq. (7) to be written as

$$\langle T(_\nu^{\boldsymbol{\kappa}}{}_\alpha^b;\omega)\rangle = \lim_{\tau_0\to\infty}\frac{1}{4\tau_0}\left|\frac{1}{\sqrt{2\pi}}\int_{-\tau_0}^{\tau_0}\dot{q}(_\nu^{\boldsymbol{\kappa}}{}_\alpha^b;t)\exp(-i\omega t)dt\right|^2. \tag{8}$$

Substituting the expression for $\dot{q}(_\nu^{\boldsymbol{\kappa}}{}_\alpha^b;t)$ [Eq. (6)] into Eq. (8), we obtain

$$\begin{aligned} \langle T(_\nu^{\boldsymbol{\kappa}}{}_\alpha^b;\omega)\rangle =& \frac{m_b|e(_\nu^{\boldsymbol{\kappa}}{}_\alpha^b)|^2}{8\pi\tau_0 N} \\ &\times\left|\int_{-\tau_0}^{\tau_0}\sum_{l}^{N}\dot{u}_\alpha(_b^l;t)\exp\left[i\boldsymbol{\kappa}\cdot\mathbf{r}_0(_0^l)-i\omega t\right]dt\right|^2, \end{aligned} \tag{9}$$

where, for brevity, the limit has been dropped.

The spectral energy density (i.e., the total system energy in the frequency domain) is

$$\Phi(\omega,\boldsymbol{\kappa}) = 2\sum_{\nu}^{3n}\sum_{\alpha,b}^{3,n}\langle T\left(\begin{smallmatrix}\boldsymbol{\kappa} & b\\ \nu & \alpha\end{smallmatrix};\omega\right)\rangle$$
$$= \frac{1}{4\pi\tau_0 N}\sum_{b}^{n} m_b \sum_{\alpha}^{3}\left|\int_{-\tau_0}^{\tau_0}\sum_{l}^{N}\dot{u}_\alpha\left(\begin{smallmatrix}l\\ b\end{smallmatrix};t\right)\exp\left[i\boldsymbol{\kappa}\cdot\mathbf{r}_0\left(\begin{smallmatrix}l\\ 0\end{smallmatrix}\right)-i\omega t\right]dt\right|^2, \tag{10}$$

where we have used the fact that the eigenvectors are orthonormal (i.e., $\sum_{\nu}^{3n}|e\left(\begin{smallmatrix}\boldsymbol{\kappa} & b\\ \nu & \alpha\end{smallmatrix}\right)|^2 = 1$) [12] and equipartition of energy (valid for a classical, harmonic system). Given the atomic velocities in a system, the spectral energy density can be calculated at arbitrary frequencies for the allowed wave vectors. The Hamiltonian can be written as

$$H = \sum_{\boldsymbol{\kappa}}^{N}\int_{-\infty}^{\infty}\Phi(\omega,\boldsymbol{\kappa})d\omega = 2\sum_{\boldsymbol{\kappa},\nu}^{N,3n}\sum_{\alpha,b}^{3,n}\langle T\left(\begin{smallmatrix}\boldsymbol{\kappa} & b\\ \nu & \alpha\end{smallmatrix};t\right)\rangle. \tag{11}$$

Relation to Phonon Properties

In an anharmonic system, the phonon populations fluctuate about the equilibrium distribution function. The phonon mode coordinates and their time derivatives are

$$q_A(\boldsymbol{\kappa}_\nu;t) = [q_{SS}(\boldsymbol{\kappa}_\nu;t) + q_T(\boldsymbol{\kappa}_\nu;t)] \tag{12}$$

and

$$\dot{q}_A(\boldsymbol{\kappa}_\nu;t) = [\dot{q}_{SS}(\boldsymbol{\kappa}_\nu;t) + \dot{q}_T(\boldsymbol{\kappa}_\nu;t)]. \tag{13}$$

The steady-state and transient parts and their time derivatives are given by

$$q_{SS}(\boldsymbol{\kappa}_\nu;t) = C_1(\boldsymbol{\kappa}_\nu)\exp\{i\omega_A(\boldsymbol{\kappa}_\nu)t\} + C_2(\boldsymbol{\kappa}_\nu)\exp\{-i\omega_A(\boldsymbol{\kappa}_\nu)t\}, \tag{14}$$

$$q_T(\boldsymbol{\kappa}_\nu;t) = \exp[-\Gamma(\boldsymbol{\kappa}_\nu)|t|]\{C_3(\boldsymbol{\kappa}_\nu)\exp[i\omega_A(\boldsymbol{\kappa}_\nu)t] - C_4(\boldsymbol{\kappa}_\nu)\exp[-i\omega_A(\boldsymbol{\kappa}_\nu)t]\}, \tag{15}$$

$$\dot{q}_{SS}(\boldsymbol{\kappa}_\nu;t) = i\omega_A(\boldsymbol{\kappa}_\nu)\left\{C_1(\boldsymbol{\kappa}_\nu)\exp[i\omega_A(\boldsymbol{\kappa}_\nu)t] - C_2(\boldsymbol{\kappa}_\nu)\exp[-i\omega_A(\boldsymbol{\kappa}_\nu)t]\right\}, \tag{16}$$

and

$$\dot{q}_T(\boldsymbol{\kappa}_\nu;t) = \exp[-\Gamma(\boldsymbol{\kappa}_\nu)|t|]\{C_3(\boldsymbol{\kappa}_\nu)[i\omega_A(\boldsymbol{\kappa}_\nu) - \Gamma(\boldsymbol{\kappa}_\nu)]\exp[i\omega_A(\boldsymbol{\kappa}_\nu)t] - C_4(\boldsymbol{\kappa}_\nu)[i\omega_A(\boldsymbol{\kappa}_\nu) + \Gamma(\boldsymbol{\kappa}_\nu)]\exp[-i\omega_A(\boldsymbol{\kappa}_\nu)t]\}, \tag{17}$$

where the Cs are constants and $\omega_A(\boldsymbol{\kappa}_\nu)$ and $\Gamma(\boldsymbol{\kappa}_\nu)$ are the phonon mode frequency and scattering rate (i.e., linewidth). The transient part describes the creation of an excess in the population of a phonon mode for $t<0$ and its decay back to equilibrium for $t>0$.

The model used for anharmonic lattice dynamics is an excitation and decay of a single phonon mode. In a real system, there will be multiple phonons in each mode that simultaneously grow or decay with time. Thus, (dealing only with $\dot{q}$) we let

$$\dot{q}(\boldsymbol{\kappa}_\nu;t) = \sum_j i\exp[-\Gamma(\boldsymbol{\kappa}_\nu)|t-t_j|] \times\{A_j(\boldsymbol{\kappa}_\nu)[\omega_A(\boldsymbol{\kappa}_\nu)+i\Gamma(\boldsymbol{\kappa}_\nu)]\exp[i\omega_A(\boldsymbol{\kappa}_\nu)(t-t_j)] - B_j(\boldsymbol{\kappa}_\nu)[\omega_A(\boldsymbol{\kappa}_\nu)-i\Gamma(\boldsymbol{\kappa}_\nu)]\exp[-i\omega_A(\boldsymbol{\kappa}_\nu)(t-t_j)]\}, \tag{18}$$

where many phonons in each mode, indexed by j, are simultaneously being created and destroyed. The phonons grow for $t<t_j$ and decay for $t>t_j$ and A_j and B_j are constants. We are not concerned with the values of t_j, A_j, and B_j, though they should take on values such that $\langle\dot{q}^*_{SS}(\boldsymbol{\kappa}_\nu;t)\,\dot{q}_{SS}(\boldsymbol{\kappa}_\nu;t)\rangle = \langle\dot{q}^*(\boldsymbol{\kappa}_\nu;t)\,\dot{q}(\boldsymbol{\kappa}_\nu;t)\rangle$.

Next, we note that

$$\langle T(\boldsymbol{\kappa}_\nu;\omega)\rangle = \sum_{\alpha,b}^{3,n}\langle T\left(\begin{smallmatrix}\boldsymbol{\kappa} & b\\ \nu & \alpha\end{smallmatrix};\omega\right)\rangle = \lim_{\tau_0\to\infty}\frac{1}{4\tau_0}\left|\frac{1}{\sqrt{2\pi}}\int_{-\tau_0}^{\tau_0}\dot{q}(\boldsymbol{\kappa}_\nu;t)\exp(-i\omega t)dt\right|^2, \tag{19}$$

which can be shown using $T(\boldsymbol{\kappa}_\nu;t)$ and $\dot{q}(\boldsymbol{\kappa}_\nu;t)$ in place of $T\left(\begin{smallmatrix}\boldsymbol{\kappa} & b\\ \nu & \alpha\end{smallmatrix};t\right)$ and $\dot{q}\left(\begin{smallmatrix}\boldsymbol{\kappa} & b\\ \nu & \alpha\end{smallmatrix};t\right)$ in Eq. (7) and using Parseval's theorem [as used to obtain Eq. (8)]. By substituting Eq. (18) into Eq. (19) and performing the integration over time we find

$$\langle T(\boldsymbol{\kappa}_\nu;\omega)\rangle = \frac{1}{16\pi\tau_0}\left|\sum_j\exp[-i\omega t_j]\left\{A_j(\boldsymbol{\kappa}_\nu)\frac{\omega_A(\boldsymbol{\kappa}_\nu)+i\Gamma(\boldsymbol{\kappa}_\nu)}{\omega_A(\boldsymbol{\kappa}_\nu)-\omega+i\Gamma(\boldsymbol{\kappa}_\nu)} + B_j(\boldsymbol{\kappa}_\nu)\frac{\omega_A(\boldsymbol{\kappa}_\nu)-i\Gamma(\boldsymbol{\kappa}_\nu)}{\omega_A(\boldsymbol{\kappa}_\nu)+\omega-i\Gamma(\boldsymbol{\kappa}_\nu)}\right\}\right|^2. \tag{20}$$

We are primarily interested in values of ω where $\omega\approx\omega_A$. When $\omega\approx\omega_A$, the term involving A_j becomes large since $\Gamma << \omega_A$ and the term involving B_j can be neglected. (Alternatively, we could ignore the term involving A_j when $\omega\approx-\omega_A$.) Hence, we find

$$\langle T(\boldsymbol{\kappa}_\nu;\omega)\rangle = \frac{1}{16\pi\tau_0}\sum_j\sum_{j'}\cos\left[\omega(t_{j'}-t_j)\right]A_j(\boldsymbol{\kappa}_\nu)A_{j'}(\boldsymbol{\kappa}_\nu) \times\frac{\omega_A^2(\boldsymbol{\kappa}_\nu)+\Gamma^2(\boldsymbol{\kappa}_\nu)}{\Gamma(\boldsymbol{\kappa}_\nu)}\frac{\Gamma(\boldsymbol{\kappa}_\nu)}{[\omega_A(\boldsymbol{\kappa}_\nu)-\omega]^2+\Gamma^2(\boldsymbol{\kappa}_\nu)}. \tag{21}$$

Using Eqs. (10), (19), and (21), we finally arrive at

$$\Phi(\omega,\boldsymbol{\kappa}) = 2\sum_{\nu}^{3n}\langle T(\overset{\boldsymbol{\kappa}}{\nu};\omega)\rangle = \sum_{\nu}^{3n} C_0(\overset{\boldsymbol{\kappa}}{\nu})\,\frac{\Gamma(\overset{\boldsymbol{\kappa}}{\nu})/\pi}{[\omega_A(\overset{\boldsymbol{\kappa}}{\nu})-\omega]^2+\Gamma^2(\overset{\boldsymbol{\kappa}}{\nu})}, \quad (22)$$

where

$$C_0(\overset{\boldsymbol{\kappa}}{\nu}) = \sum_j\sum_{j'}\cos\left[\omega(t_{j'}-t_j)\right]A_j(\overset{\boldsymbol{\kappa}}{\nu})A_{j'}(\overset{\boldsymbol{\kappa}}{\nu})\,\frac{\omega_A^2(\overset{\boldsymbol{\kappa}}{\nu})+\Gamma^2(\overset{\boldsymbol{\kappa}}{\nu})}{8\tau_0\Gamma(\overset{\boldsymbol{\kappa}}{\nu})}. \quad (23)$$

Thus, $\Phi(\omega,\boldsymbol{\kappa})$ is a superposition of $3n$ Lorentzian functions with centers at $\omega_A(\overset{\boldsymbol{\kappa}}{\nu})$ with a half-width at half-maximum of $\Gamma(\overset{\boldsymbol{\kappa}}{\nu})$. We know from anharmonic LD that [7, 10]

$$\tau(\overset{\boldsymbol{\kappa}}{\nu}) = \frac{1}{2\Gamma(\overset{\boldsymbol{\kappa}}{\nu})}, \quad (24)$$

where τ is the phonon relaxation time.

Once the frequencies and relaxation times of all phonon modes in the Brillouin zone are obtained, the bulk thermal conductivity in direction $\mathbf{n}$, $k_{\mathbf{n}}$, can be calculated from

$$k_{\mathbf{n}} = \sum_{\boldsymbol{\kappa}}\sum_{\nu} c(\overset{\boldsymbol{\kappa}}{\nu})\,v_{g,\mathbf{n}}^2(\overset{\boldsymbol{\kappa}}{\nu})\,\tau(\overset{\boldsymbol{\kappa}}{\nu}). \quad (25)$$

Here, c is the phonon volumetric specific heat and $v_{g,\mathbf{n}}$ is the component of the group velocity vector in direction $\mathbf{n}$. The specific heat can be obtained using the Bose-Einstein distribution for phonons, which requires the frequencies [20]. The group velocity vector is the gradient of the dispersion curves (i.e., $\partial\omega/\partial\boldsymbol{\kappa}$, see Fig. 1) and thus also requires the frequencies.

LENNARD-JONES ARGON CASE STUDY

We now use molecular dynamics (MD) simulation and the SED method to predict the properties of phonons along the [100] direction in Lennard-Jones argon. We consider a temperature of 20 K for which the zero-pressure lattice constant, a, is 5.315 Å [3]. The MD system consists of $4\times4\times4$ conventional unit cells for a total of 256 atoms. Using a 5 fs time step, the system is equilibrated for 5 ns before collecting data every time step for an additional 10 ns. The results of five independent simulations (with different initial conditions) are then averaged. We also average over the [100], [010], and [001] directions.

The results are plotted in Fig. 1. In the topmost sub-figure, the dispersion curves, as predicted from quasi-harmonic LD, are shown. While dispersion is normally plotted as frequency versus wave vector magnitude, here we invert the axes for convenience. In the three remaining sub-figures the SED is plotted versus frequency for wave vectors along the [100] direction with magnitudes of π/a, $\pi/2a$, and 0. The modes indicated with open circles on the dispersion curves can be seen as peaks in the SED plots. The peaks below 10 rad/ps are well defined. The peaks at higher frequencies are noisier.

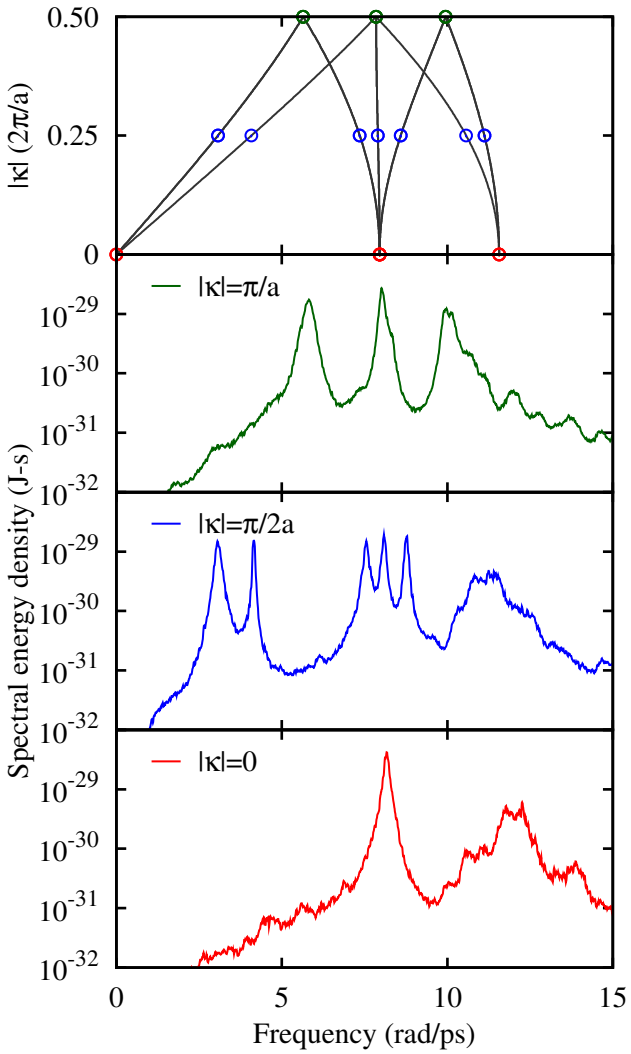

FIGURE 1. DISPERSION CURVES ALONG THE [100] DIRECTION AND THE SPECTRAL ENERGY DENSITY VERSUS FREQUENCY FOR WAVE VECTORS ALONG THE [100] DIRECTION WITH MAGNITUDES OF π/a, $\pi/2a$, AND 0 FOR LENNARD-JONES ARGON AT A TEMPERATURE OF 20 K. THE MODES INDICATED WITH OPEN CIRCLES ON THE DISPERSION CURVES CAN BE SEEN AS PEAKS IN THE SPECTRAL ENERGY DENSITY PLOTS. THE ZERO FREQUENCY, ZERO WAVE VECTOR MODE CORRESPONDS TO BULK TRANSLATION AND DOES NOT EXIST IN MD SIMULATIONS WITH ZERO TOTAL MOMENTUM. THE DATA IS SMOOTHED FOR VISUALIZATION BUT THE LORENTZIAN FUNCTIONS ARE FIT TO THE RAW DATA.

By fitting the peaks in the SED with Lorentzian functions

TABLE 1. LENNARD-JONES ARGON PHONON PROPERTIES PREDICTED BY THE SPECTRAL ENERGY DENSITY METHOD (SED), NORMAL-MODE DECOMPOSITION (NMD), AND ANHARMONIC LATTICE DYNAMICS CALCULATIONS (ALD) AT A TEMPERATURE OF 20 K.

	SED		MND		ALD	
$\lvert\boldsymbol{\kappa}\rvert$	ω_A (1/ps)	τ (ps)	ω_A (1/ps)	τ (ps)	ω_A (1/ps)	τ (ps)
0	8.17	6.02	8.16	5.15	8.20	12.7
	12.0	1.10	12.0	1.36	12.0	1.45
$\frac{\pi}{a}$	3.07	5.45	3.06	7.43	3.11	6.74
	4.15	13.9	4.15	8.85	4.24	15.3
	7.55	6.43	7.55	5.20	7.59	10.3
	8.09	8.09	8.08	5.43	8.12	14.0
	8.77	8.82	8.77	4.62	8.81	16.5
	10.8	3.21	10.8	1.93	10.9	2.60
	11.4	1.19	11.4	1.29	11.4	1.57
$\frac{\pi}{2a}$	5.81	3.32	5.80	4.28	5.83	6.68
	8.02	6.89	8.02	5.51	8.06	14.7
	8.21	4.29	8.07	5.44	8.13	10.9
	10.0	2.47	10.0	2.58	10.1	4.19

using a least squares method, we can extract the phonon frequencies and relaxation times [see Eq. (22)]. The results are tabulated in Table 1 for all unique (i.e., non-degenerate) modes. The table also includes predictions made using the normal-mode decomposition MD method [3] and anharmonic LD calculations [13]. The normal-mode decomposition predictions are made using the same simulations as those used for the SED. The agreement between the SED method and the normal-mode decomposition method is generally good, as it should be since these methods are similar. In both methods, the system energy is being mapped from direct space and time to reciprocal space and frequency. The agreement with the anharmonic LD predictions is not as good. This result may be due to the low temperature approximations inherent in LD techniques [13]. The normal-mode decomposition method also loses accuracy at higher temperatures because the quasi-harmonic phonon frequencies and polarization vectors are used to perform the energy mapping [13]. The SED method, however, does not suffer from this limitation and should be applicable at higher temperatures as long as the weakly-interacting phonon interpretation is valid.

SUMMARY

In this paper, we derived the spectral energy density and the relationship between the spectral energy density and the phonon frequencies and relaxation times. We then calculated the spectral energy density for Lennard-Jones argon at a temperature of 20 K and used it to obtain the phonon frequencies and relaxation times, as shown in Fig. 1 and Table 1. The frequencies are in excellent agreement with those predicted using other techniques, while the relaxation times show reasonable agreement. Further work is required to understand the differences.

The advantages of the SED method are that (i) other than the the wave vectors, which can be determined from the system geometry, no phonon properties need to be known *a priori* and (ii) it naturally incorporates the full effect of anharmonicity (through the MD simulation). The main disadvantage is that the different dispersion branches are not handled separately. Instead, the SED at each wave vector contains information for all dispersion branches. As a result, it can be difficult to identify or fit Lorentzian functions to closely-spaced peaks in the SED. Though not essential, knowledge of the quasi-harmonic frequencies can help to identify the unique peaks in the SED as well as the degeneracy.

ACKNOWLEDGMENT

This work is supported by the Pennsylvania Infrastructure Technology Alliance, a partnership of Carnegie Mellon, Lehigh University, and the Commonwealth of Pennsylvania's Department of Community and Economic Development (DCED), Advanced Micro Devices (AMD), and the National Science Foundation through a graduate fellowship to JAT.

REFERENCES

[1] Callaway, J., 1959. "Model for lattice thermal conductivity at low temperatures". *Physical Review,* ***113***, p. 1046.

[2] Holland, M. G., 1963. "Analysis of lattice thermal conductivity". *Physical Review,* ***132***, p. 2461.

[3] McGaughey, A. J. H., and Kaviany, M., 2004. "Quantitative validation of the Boltzmann transport equation phonon thermal conductivity model under the single-mode relaxation time approximation". *Physical Review B,* ***69***, p. 094303.

[4] Landry, E. S., Hussein, M. I., and McGaughey, A. J. H., 2008. "Complex superlattice unit cell designs for reduced thermal conductivity". *Physical Review B,* ***77***, p. 184302.

[5] Schelling, P. K., Phillpot, S. R., and Keblinski, P., 2002. "Comparison of atomic-level simulation methods for computing thermal conductivity". *Physical Review B,* ***65***, p. 144306.

[6] Sellan, D. P., Landry, E. S., Turney, J. E., McGaughey, A. J. H., Amon, C. H., and McGaughey, A. J. H., 2010. "Size

effects in molecular dynamics thermal conductivity prediction". *Physical Review B,* ***81***, p. 214305.

[7] Ladd, A. J. C., Moran, B., and Hoover, W. G., 1986. "Lattice thermal conductivity: A comparison of molecular dynamics and anharmonic lattice dynamics". *Physical Review B,* ***34***, pp. 5058–5064.

[8] Henry, A. S., and Chen, G., 2008. "Spectral phonon transport properties of silicon based on molecular dynamics simulations and lattice dynamics". *Journal of Computational and Theoretical Nanoscience,* ***5***, pp. 1–12.

[9] Goicochea, J. V., Madrid, M., and Amon, C. H., 2010. "Thermal properties for bulk silicon based on the determination of relaxation times using molecular dynamics". *Journal of Heat Transfer,* ***132***, p. 012401.

[10] Maradudin, A. A., and Fein, A. E., 1962. "Scattering of neutrons by an anharmonic crystal". *Physical Review,* ***128***, pp. 2589–2608.

[11] Wallace, D. C., 1972. *Thermodynamics of Crystals*. Cambridge Univ. Press, Cambridge, UK.

[12] Dove, M. T., 1993. *Introduction to Lattice Dynamics*. Cambridge, Cambridge.

[13] Turney, J. E., Landry, E. S., McGaughey, A. J. H., and Amon, C. H., 2009. "Predicting phonon properties and thermal conductivity from anharmonic lattice dynamics calculations and molecular dynamics simulations". *Physical Review B,* ***79***, p. 064301.

[14] Marayuma, S., 2003. "A molecular dynamics simulation of heat conduction of a finite length single-walled carbon nanotube". *Nanoscale and Microscale Thermophysical Engineering,* ***7***, pp. 41–50.

[15] Shiomi, J., and Maruyama, S., 2006. "Non-fourier heat conduction in a single-walled carbon nanotube: Classical molecular dynamics simulations". *Phys. Rev. B,* ***73***, p. 205420.

[16] de Koker, N., 2009. "Thermal conductivity of MgO periclase from equilibrium first principles molecular dynamics". *Physical Review Letters,* ***103***, p. 125902.

[17] Thomas, J. A., Turney, J. E., Iutzi, R. M., Amon, C. H., , and McGaughey, A. J. H., 2010. "Predicting phonon dispersion relations and lifetimes from the spectral energy density". *Physical Review B,* ***81***, p. 081411(R).

[18] Turney, J. E., 2009. "Predicting phonon properties and thermal conductivity using anharmonic lattice dynamics calculations". PhD Thesis, Carnegie Mellon University, Pittsburgh, PA.

[19] Rudin, W., 1987. *Real and Complex Analysis*. McGraw-Hill, New York.

[20] Srivastava, G. P., 1990. *The Physics of Phonons*. Adam Hilger, Bristol.